LOW-DIMENSIONAL SYSTEMS

Structure and Properties of Nanocomposite Nb–Al–N films

**V. I. Ivashchenko[a], A. D. Pogrebnjak[b, *], O. V. Sobol'[c], P. L. Skrynskii[a], V. N. Rogoz[b],
A. A. Meilekhov[c], S. N. Dub[d], and A. I. Kupchishin[e]**

[a] Frantsevich Institute for Problems of Materials Science, National Academy of Sciences of Ukraine,
str. Kryzhanovskogo 3, Kyiv, 03680 Ukraine

[b] Sumy State University, ul. Rimskogo-Korsakova 2, Sumy, 40007 Ukraine

* e-mail: alexp@i.ua

[c] National Technical University "Kharkiv Polytechnic Institute," ul. Frunze 21, Kharkiv, 61002 Ukraine

[d] Bakul Institute for Superhard Materials, National Academy of Sciences of Ukraine,
str. Avtozavodskaya 2, Kyiv, 04074 Ukraine

[e] Kazakh National Pedagogical University named after Abai,
pr. Dostyk 13, Almaty, 050010 Kazakhstan

Received January 27, 2015; in final form, February 6, 2015

Abstract—Nanocomposite Nb–Al–N films prepared by magnetron sputtering have been studied. It has been found that, in the films, there are two stable crystalline structural states, namely, NbN_z and $B1–Nb_{1-x}Al_xN_yO_{1-y}$, and an amorphous-like component related to aluminum oxynitride upon reactive magnetron sputtering. It has been established that the substructure characteristics are sensitive to the current supplied to an Al target and are related to the Knoop nanohardness and hardness, which change in the ranges of 29–33.5 and 46–48 GPa, respectively. Ab initio calculations for the NbN_z and Nb_2AlN phases and NbN/AlN heterostructures have been performed to interpret the obtained results for the first time.

1. INTRODUCTION

Films based on NbN demonstrate a variety of interesting properties, such as high hardness, electrical conductivity, thermal stability, and chemical inertness [1]. The NbN films are used as cathode materials for the field emission under vacuum in microelectronic devices [2]. It was shown that introduction of Al atoms into the crystal lattice leads to the formation of $Nb_{1-x}Al_xN$ solid solutions. The Nb–Al–N films consist of $Nb_{1-x}Al_xN$ solid solutions with the $B1$ (rarely, B_K, which is the δ'-NbN phase) and $B4$ structures or their mixtures [3–7]. In $Nb_{1-x}Al_xN$ solid solutions, the $B1$ structure is more preferable at aluminum concentrations x lower than 0.45. In the range from $x = 0.45$ to 0.71, a mixture of $B1$ and $B4$ structures is observed, while at $x > 0.71$, the $B4$ structure (wurtzite type with a hexagonal structure) is formed [6, 7]. On the other hand, nanocomposite NbN/AlN films have not yet been studied up to now. Thus, the aim of this work was to study Nb–Al–N films, because nanocomposite structures of films with higher mechanical properties as compared to those of films consisting of substitutional $Nb_{1-x}Al_xN$ solid solutions can be formed under specific conditions.

## 2. SAMPLE PREPARATION AND EXPERIMENTAL TECHNIQUE

The Nb–Al–N films were deposited on specularly polished Si(100) plates using a magnetron dc sputtering of Nb (99.9%) and Al (99.999%) 4-mm-thick targets 72 mm in diameter in argon and nitrogen atmospheres with the following deposition parameters: substrate temperature $T_S = 350°C$, bias voltage at the substrate $U_B = -50$ V, flow rates $F_{Ar} = 40$ cm³/min, $F_{N_2} = 13$ cm³/min, and operating pressure $p = 0.17$ Pa. The currents supplied to the Al target were $I_{Al} = 100, 150, 200, 250,$ and 300 mA, which corresponded to the discharge power densities $P_{Al} = 5.7, 8.6, 11.4, 13.7,$ and 17.1 W/cm². The current supplied to the Nb target was $I_{Nb} = 300$ mA ($P_{Nb} = 17.1$ W/cm²). The base pressure in the vacuum chamber was lower than 10^{-4} Pa. The distance between the target and the target holder was 8 cm. The dihedral angle between the targets was ~45°. The substrates were cleaned by ultrasonic treatment before placing them into the chamber. In addition, the substrates were etched in the vacuum chamber in a hydrogen plasma for 5 min before the deposition.

The structural and mechanical properties were analyzed as functions of I_{Al}. The coating structure was studied using X-ray diffraction (XRD, Dron-3M diffractometer, CuK_α radiation). When the complex dif-

fraction profiles were superposed, they were separated using the program developed by the authors. The substructure characteristics (crystallite size and microstrain) were determined by an approximation method using the Cauchy function as the approximating function. The Fourier spectra were measured on a TSM 1202 (LTD Infraspek) spectrometer in the range of $400{-}4000$ cm^{-1} at room temperature. The Knoop hardness (HK) was estimated using a Microhardness Tester Micromet 2103 BUEHLER LTD at a load of 100 mN, as well as by the nanoindentation using a G-200 nanohardness tester equipped with a Berkovich indenter. Loads were chosen based on the following condition: the indenter penetration should be not higher than $10{-}20\%$ of the film thickness. The elastic modulus was measured in a dynamic mode on a Triboindenter TI-950 (HYSITRON) apparatus. The film thickness was determined using a "Micron-gamma" optic profilometer. The thickness of Nb–Al–N coatings d weakly depended on I_{Al}. The values of d were in the range of $0.7{-}0.9$ μm.

3. RESULTS AND DISCUSSION

Figure 1a shows the X-ray diffraction patterns of the Nb–Al–N films at different currents I_{Al}. The marked peaks correspond to the $B1$-NbN$_z$ structure [8]. The patterns demonstrate a halo-like component from an amorphous phase in the diffraction angle range $2\theta = 18°{-}30°$; the component can be identified as the aluminum nitride amorphous phase based on previous studies. It is seen that reflection (200) is the main reflection. It follows that crystallites with the dominant growth orientation along axis [100] perpendicular to the surface plane are formed at all I_{Al} and a relatively low constant bias potential on the substrate of -50 V. The X-ray diffraction patterns show that reflections (200) and (400) are asymmetric (to the side of larger angles). Separation of these reflection profiles shows the existence of two components with similar types of the crystal lattices but two characteristic lattice parameters. Figure 1b shows the result of the deconvolution of the peaks (200) and (400) into Gaussians for the film deposited at 150 mA (Fig. 1a, curve 2). In Fig. 1b, curves 1 correspond to cubic niobium nitride with lattice parameter $a = 0.439{-}0.438$ nm. Gaussian curve 2 can be assigned to a cubic NbN with a low content of substituting aluminum with $a = 0.428{-}0.429$ nm, which is characteristic of the Nb–Al–N system with the proportion of aluminum and niobium atoms in the crystal lattice of 1/2 (approximate composition Nb$_{0.67}$Al$_{0.33}$N). The latter was determined based on the Vegard's law for one-type crystal lattices when substituting atoms of different radii [9]. In this case, the base lattice parameters are 0.4393 and 0.4120 nm for $B1$-NbN$_z$ and $B1$-AlN, respectively. As I_{Al} increases, the Gaussian peak positions are almost unchanged but the peak intensities increase. At high
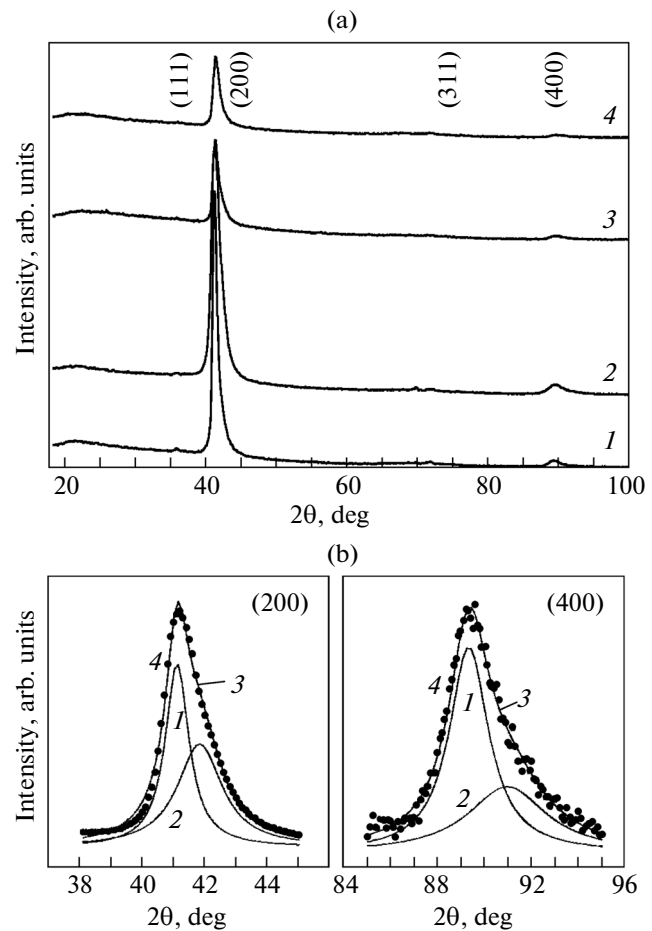
Fig. 1. (a) X-ray diffraction patterns of the Nb–Al–N coatings deposited at $I_{Al} = $ (1) 100, (2) 150, (3) 250, and (4) 300 mA. (b) A fragment with separation into components of the diffraction profile of the Nb–Al–N coatings deposited at $I_{Al} = 150$ mA: (1) NbN$_z$, (2) Nb$_{0.67}$Al$_{0.33}$N, (3) total approximating curve, and (4) points of the initial data array.

currents, the proportion of the NbN$_z$/Nb$_{0.67}$Al$_{0.33}$N phases is almost 3/5.

To determine the substructure characteristics, we used the method of approximation of two orders of the diffraction reflections. We used the (200)–(400) pair. The results of determining the substructure characteristics are shown in Fig. 2. It is seen that the crystallite size and the microstrain increase in the direction of the [100] texture axis for both NbN$_z$ crystallites (dependences 1 in Fig. 2) and crystallites of the Nb$_{0.67}$Al$_{0.33}$N phase (dependences 2 in Fig. 2) as current I_{Al} increases. The sharp decrease in the crystallite size and the microstrain at the highest current $I_{Al} = 300$ mA can be due to the annealing and the ordering of the defect structure with the formation of new boundaries by type of the polygonization process. A higher microstrain in Nb$_{0.67}$Al$_{0.33}$N crystallites (dependence 2 in Fig. 2b) is likely determined by dis-
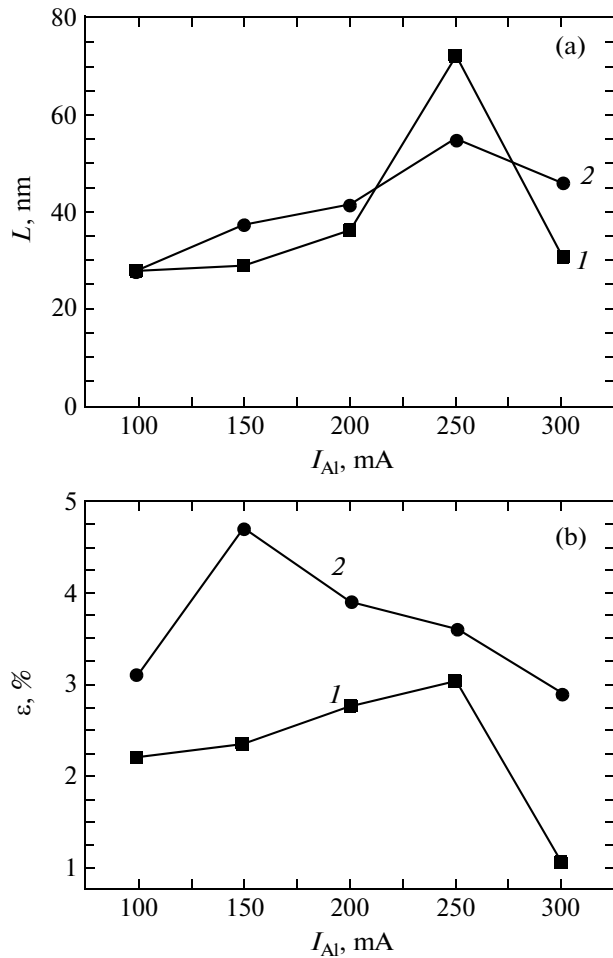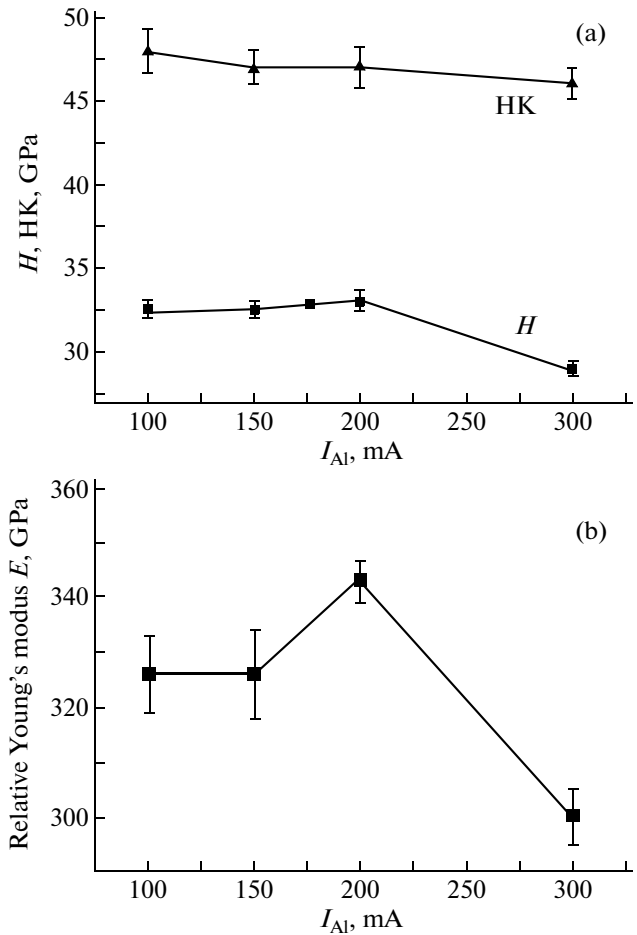
Fig. 2. Dependences of the substructure characteristics (a) average crystallite size L and (b) microstrain ε on I_{Al} for different crystalline components: (1) NbN_z, (2) $Nb_{0.67}Al_{0.33}N$ (or Nb_2AlN).

Fig. 3. (a) Nanohardness (H), Knoop hardness (HK), and (b) elastic modulus (E) as functions of I_{Al} for the $Nb_{0.67}Al_{0.33}N$ coatings.

solution of aluminum atoms in the niobium lattice, which strongly distorts the lattice.

We deposited AlN films at different currents I_{Al}. The X-ray diffraction patterns show that all the AlN films are amorphous (α-AlN, the patterns are not shown in this work). The infrared absorption spectra of the AlN films show that the number of the Al–N bonds increases with I_{Al} (the absorption band at 667 cm^{-1} related to the Al–N vibrations [10] becomes more noticeable).

Based on these results, it can be suggested that the films have two stable crystalline structural states: $B1$-NbN_z and a solid solution with the composition close to $B1$-$Nb_{0.67}Al_{0.33}N$. The films also contain an amorphous-like component related to aluminum nitride. Thus, the films exhibit a nanocomposite structure and consist of $B1$-NbN_z and $B1$-$Nb_{1-x}Al_xN$ nanocrystallites introduced into the a-AlN matrix.

The results of nanoindentation and microindentation of the films deposited are shown in Fig. 3. A comparison of the results presented in Figs. 2 and 3 shows that there is a correlation between the mechanical characteristics and the microstrains in the Nb–Al–N films. The nanohardness, the elastic modulus, and the Knoop hardness are maximal in the Nb–Al–N films with grain sizes of 30–40 nm. The increase in the nanohardness from 28 GPa in the NbN film [11] to 32 GPa in the Nb–Al–N films is likely due to the formation of a nanocomposite structure of this film. We find that the Knoop hardness is ~50% higher than the nanohardness. This circumstance can be due to that the nanoindentation is performed in a dynamic mode, while the Knoop hardness is determined at static conditions.

In order to verify our conclusions on the structure of the Nb–Al–N films, we performed ab initio calculations for $B1$-NbN_z, solid solutions $B1$-$Nb_{1-x}Al_xN$, heterostructures $B1$-$NbN(001)/B1$-AlN, and ordered phase Nb_2AlN. The calculation conditions are

$E(a) - E(b) = +0.016$ eV/atom
$E(c) - E(d) = -0.039$ eV/atom
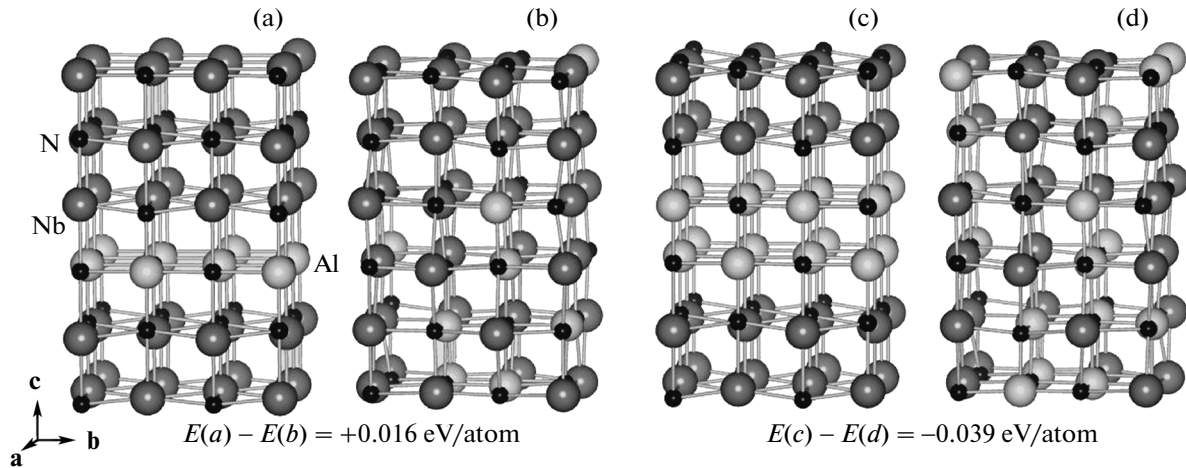
Fig. 4. Atomic configurations of (a) heterostructure $B1$-NbN_z (001)/1 ML $B1$-AlN, (b) solid solution $Nb_{0.83}Al_{0.17}N$, (c) heterostructure $B1$-NbN_z (001)/2 ML $B1$-AlN, and (d) solid solution $Nb_{0.67}Al_{0.33}N$. The structures shown in panels (a) and (b) have the same composition; the composition of the structure shown in panel (c) is equal to that of the heterostructure shown in panel (d). Shown at the bottom are the differences between the total energies of the heterostructure and the corresponding solid solution with a chaotic arrangement of atoms in the metal lattice.

described in detail in [12]. Note that the calculations were performed using a computational code [13]. We used the generalized gradient approximation for the exchange−correlation potential [14]. The molecular dynamics simulation was carried out using the *NVT* (canonical) ensemble at 1400 K with subsequent cooling to 0 K and static relaxation [12]. We considered 96-atom structures constructed by translation of a $(2 \times 2 \times 3)$ $B1$ cell [12]. The compositions of the solid solutions and the heterostructures were chosen to be the same. The Nb_2AlN unit cell (space group $P6_3/mmc$, N 194) consists of eight atoms.

The structures under consideration include all possible configurations of the $Nb_{1-x}Al_xN$ system. The X-ray diffraction patterns were considered using the PowderCell-2.4 program software [15].

Figure 4 shows the atomic configurations of heterostructures $B1$-NbN_z (001)/1 ML, $B1$-AlN and $B1$-NbN_z (001)/2 ML $B1$-AlN (ML is for monolayer), and also solid solutions $B1$-$Nb_{1-x}Al_xN$. An analysis of the total energies shows that the $B1$-$Nb_{1-x}Al_xN$ solid solutions with $x < 0.33$ should decompose, and a nanocomposite structure with $B1$-AlN interface can are formed at these concentrations x. Using the atomic configurations obtained as a result of the ab initio calculations, we calculated the X-ray diffraction patterns for $B1$-NbN_z, $B1$-$Nb_{1-x}Al_xN$ ($x \sim 0.33$), and Nb_2AlN. The calculated X-ray diffraction patterns are shown in Fig. 5. A comparison of the calculated and the experimental data (Fig. 1) shows that the experimental X-ray diffraction patterns do not contain reflections near $2\theta \sim 32°$ related to the heterostructure and near $2\theta \sim 38°$ due to the Nb_2AlN phase. Because of this, we can assume that our films do not contain either Nb_2AlN or

epitaxial layers $B1$-AlN, and consist, most likely, of crystallites $B1$-NbN_z and $B1$-$Nb_{1-x}Al_xN$ ($x \sim 0.33$). This conclusion is also supported by the fact that the difference of the peak positions $\Delta 2\theta = 2\theta(B1$-$NbN_z) - 2\theta(B1$-$Nb_{1-x}Al_xN)$ in the experimental and the theoretical X-ray diffraction patterns are almost the same for each of diffraction peaks (200) and (400). Here, it also should be noted that the niobium nitride-based films are prone to accumulate a small oxygen amount [5]. Oxygen can replace a part of nitrogen in the solid solutions and in the amorphous matrix [16, 17]. Because of this, a more reliable structure of the solid solutions is $Nb_{1-x}Al_xN_yO_{1-y}$ ($x \sim 0.33$; $(1 - y) \ll 1$) and that of the amorphous phase is a-AlNO, which was shown as a result of the elemental analysis per-
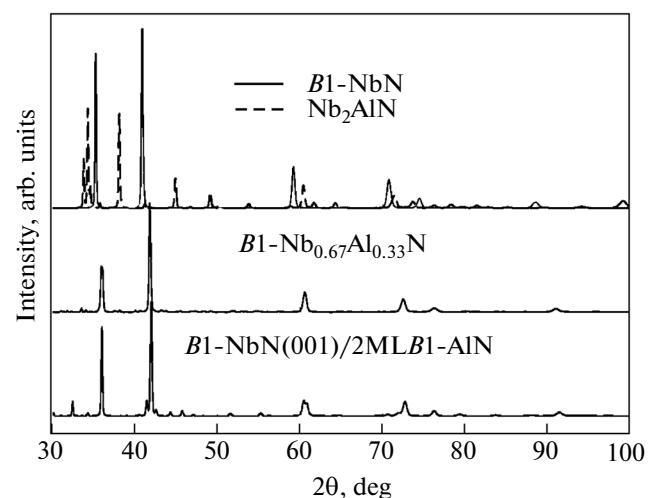
Fig. 5. Calculated X-ray diffraction patterns.

formed for these films using mass-spectroscopy of secondary ions, Rutherford backscattering spectroscopy, and energy-dispersive X-ray spectroscopy.

4. CONCLUSIONS

Thus, we studied the Nb–Al–N films deposited on silicon substrates by magnetron sputtering of Nb and Al targets at different discharge powers on the Al targets. The experimental and theoretical studies showed that the films prepared using the chosen deposition parameters have a nanocomposite structure and consist of nanocrystallites $B1$-NbN$_z$ and $B1$-Nb$_{1-x}$Al$_x$N$_y$O$_{1-y}$ embedded in the a-AlNO matrix. The nanocomposite coating demonstrates high values of hardness (to 32 GPa) as a result of microstrains due to the difference between the atomic radii of the metallic components of the crystal lattices. Taking into account the mechanical properties of the deposited nanocomposite films, these films can be recommended as wear-resistant and protective coatings.

ACKNOWLEDGMENTS

REFERENCES

1. S. A. Barnett, A. Madan, I. Kom, and K. Martin, MRS Bull. **28**, 169 (2003).

2. Y. Gotoh, M. Nagao, T. Ura, H. Tsuji, and J. Ishikawa, Nucl. Instrum. Methods Phys. Res., Sect. B **148**, 925 (1999).

3. T. I. Selinder, D. J Miller, and K. E. Gray, Vacuum **46**, 1401 (1995).

4. Y. Makino, K. Saito, Y. Murakami, and K. Asami, Solid State Phenom. **127**, 195 (2007).

5. H. C. Barshilla, B. Deepthi, and K. S. Rajam, J. Mater. Res. **23**, 1258 (2008).

6. R. Franz, M. Lechthaler, C. Polzer, and C. Mitterer, Surf. Coat. Technol. **204**, 2447 (2010).

7. D. Holec, R. Franz, P. H. Mayrhofer, and C. Mitterer, J. Phys. D: Appl. Phys. **41**, 145403 (2010).

8. *X-Ray Powder Diffraction File* [038-1155].

9. Ya. S. Umanskii and Yu. A. Skakov, *Physics of Metals: Atomic Structures of Metals and Alloys* (Atomizdat, Moscow, 1978) [in Russian].

10. K. Jadannadham, A. K. Sharma, Q. Wei, R. Kalyanraman, and J. Narayan, J. Vac. Sci. Technol., A **16**, 2804 (1998).

11. V. I. Ivashchenko, S. Veprek, P. L. Scrynskyy, O. Lytvyn, O. O. Butenko, O. K. Sinelnichenko, L. Gorb, F. Hill, J. Leszczynski, and A. O. Kozak, J. Superhard Mater. **36**, 1 (2014).

12. V. I. Ivashchenko, S. Veprek, P. E. A. Turchi, and V. I. Shevchenko, Phys. Rev. B: Condens. Matter **85**, 195403 (2012).

13. P. Giannozzi, S. Baroni, N. Bonini, M. Calandra, R. Car, C. Cavazzoni, D. Ceresoli, G. L. Chiarotti, M. Cococcioni. I. Dabo, A. Dal Corso, S. de Gironcoli, S. Fabris, G. Fratesi, R. Gebauer, U. Gerstmann, C. Gougoussis, A. Kokalj, M. Lazzeri, L. Martin-Samos, N. Marzari, F. Mauri, R. Mazzarello, S. Paolini, A. Pasquarello, L. Paulatto, C. Sbraccia, S. Scandolo, G. Sclauzero, A. P. Seitsonen, A. Smogunov, P. Umari, and R. M. Wentzcovitch, J. Phys.: Condens. Matter **21**, 395502 (2009).

14. J. P. Perdew, K. Burke, and M. Ernzerhof, Phys. Rev. Lett. **77**, 3865 (1996).

15. W. Kraus and G. Nolze, *PowderCell for Windows, Version 2.4* (Federal Institute for Materials Research and Testing, Berlin, 2000).

16. V. Ivashchenko, S. Veprek, A. Pogrebnjak, and B. Postolnyi, Sci. Technol. Adv. Mater. **15**, 025007 (2014).

17. A. D. Pogrebnyak, A. A. Bagdasaryan, I. V. Yakushchenko, and V. M. Beresnev, Russ. Chem. Rev. **83**, 1027 (2014).

Translated by Yu. Ryzhkov